ELSEVIER

Journal of Non-Crystalline Solids 304 (2002) 217–223

JOURNAL OF NON-CRYSTALLINE SOLIDS

www.elsevier.com/locate/jnoncrysol

Section 4. Optical properties and thin films

Luminescence properties of nanocrystalline CdS and CdS:Mn^{2+} doped silica-type glasses

Vilma C. Costa *, Yongrong Shen, Kevin L. Bray

Department of Chemistry, Washington State University, Pullman, WA 99164-4630, USA

Abstract

In the present work, we report our results for the sol–gel preparation and optical properties of CdS nanometer sized particles and Mn^{2+}-doped CdS particles in silica-type glass matrices. Gels containing 4.5 wt.% CdO in $95.5SiO_2$ and $4.5Na_2O$–$18B_2O_3$–$73.5SiO_2$ matrices were prepared through a hydrolysis of tetraethoxysilane, cadmium acetate and, in the sodium borosilicate composition, boron ethoxide and sodium acetate. We designed several heat treatments in H_2S to convert CdO to CdS in the gels. The influence of the heat treatment conditions on the optical properties of the nanoparticle semiconductor materials was studied using transmission electron microscopy, absorption, and temperature-dependent photoluminescence. A model of the photoluminescence processes was proposed to explain the observed emission bands.

PACS: 81.20.Fw; 78.67.Bf; 78.55.Et

1. Introduction

Polycrystalline semiconductors composed of nanometer sized crystallites have recently attracted interest because of their properties that result from spatial quantum confinement and their potential range of technological applications [1–4].

Among nanocrystalline semiconductors, studies of cadmium sulfide (CdS) have been done because of its relatively large nonlinear optical response [5] and photocatalytic activity [6] which are technologically relevant to optoelectronic devices [1,7], optical data storage [1], and high-speed optical communications [7,8]. Similarly, attention has been given to the mixed $Cd_{1-x}Zn_xS$ [9], $Cd_{1-x}Mn_xS$, and CdS_xSe_{1-x} nanoparticle systems [3,10,11] because of their suitability for optical devices from the near-ultraviolet to the near-infrared [12,13]. Recently, spectroscopic studies of transition-metal and rare-earth doped nanocrystalline CdS have been motivated by an effort to develop new and more efficient multicolor phosphor materials [14].

Since the properties of CdS and related nanoparticle materials are dependent on the size, shape, and composition of particles, effort has been directed toward developing processing techniques for obtaining better control of the size and distribution of nanoparticles [15–17]. These techniques include chemical colloid techniques, reverse micelle techniques [9,18,19], sol–gel process [20], hydrothermal

* Corresponding author. Address: Center of Nuclear Technology Development/CNEN, CP 941, Pampulha, CEP 30123-970, Belo Horizonte, MG Brazil. Tel.: +55-31 3499 3235; fax: +55-31 3499 3390.

E-mail address: vilma@urano.cdtn.br (V.C. Costa).

0022-3093/02/$ - see front matter
PII: S0022-3093(02)01026-8

microemulsion techniques [21], and polymerization processes [22]. The sol–gel process is one promising technique for practical applications because of size control and uniform size distribution in a low-temperature processing environment.

In this paper, we investigate CdS nanoparticles and Mn^{2+}-doped CdS nanoparticles dispersed in silica (SiO_2) and sodium borosilicate (Na_2O–B_2O_3–SiO_2) glass matrices prepared by the sol–gel process. The prepared CdS nanoparticle materials are characterized by transmission electron microscopy (TEM), optical absorption, and photoluminescence (PL) spectroscopy. We also discuss the influence of heat treatment conditions on the properties of CdS and CdS:Mn^{2+} nanoparticle materials.

2. Experimental procedure

2.1. Sample preparation

We have prepared two groups of CdS-contained glasses, silica and sodium borosilicate, by the use of the sol–gel technique [20].

Silica gels containing 4.5–5.0 wt.% CdO were prepared by hydrolysis of $Si(OC_2H_5)_4$ (TEOS), and $Cd(CH_3COO)_2 \cdot 2H_2O$ ($Cd(OAc)_2 \cdot 2H_2O$). The $Si(OC_2H_5)_4$ was first partially hydrolyzed in a mixed solution of H_2O, C_2H_5OH (TEOS/H_2O/EtOH = 1/1/1) and enough HCl to achieve an initial solution pH of 1.5–2.0. After the solution was stirred for 1 h, $Cd(OAc)_2 \cdot 2H_2O$, previously dissolved in CH_3OH, was added to it and the resulting solution was stirred for 1 h at room temperature. For samples doped with Mn^{2+}, manganese acetate was also added at this point of synthesis. The solution was next hydrolyzed by adding a mixed solution of H_2O, C_2H_5OH, and NH_4OH in a 4:1:0.01 mol per mol of TEOS. After stirring for 45 min, the sols were cast into plastic vials. After gelation, the samples were aged at 60 °C for 2 days and then dried at 90 °C for 2 days.

In a similar approach, sodium borosilicate gels containing CdO were prepared by using TEOS, boron-triethoxide, $B(OEt)_3$, and sodium acetate (CH_3CO_2Na) as starting reagents. First, TEOS was hydrolyzed in an aqueous solution (pH = 1.5) in the molar ratio TEOS:H_2O = 1:2. After the solution was stirred for 1 h, $B(OEt)_3$ was added and stirring was continued for 1 h. An aqueous solution of CH_3CO_2Na and $Cd(OAc)_2 \cdot 2H_2O$ (TEOS/H_2O = 1/4) was then added to the alkoxide mixture. For samples doped with Mn^{2+}, manganese acetate was also added at this point of synthesis. After 30 min stirring time, the resultant homogeneous solution was cast into plastic containers. The solution gelled at room temperature. After gelation, the samples were aged at 60 °C for 2 days and then dried at 90 °C for 2 days.

After drying at 90 °C, all gels were first heated to 420 °C for 24 h in O_2 to oxidize $Cd(OAc)_2$. To investigate the influence of further heat-treatment on the final material, the heated gels were subjected to one of three heat-treatment steps: exposure to H_2S gas at 150 °C for 12 h, exposure to H_2S gas at 150 °C for 4 h, or exposure to H_2S gas at 400 °C for 4 h. Some of gels produced by each of the heat treatment steps were densified at 550 °C in vacuum. Table 1 presents the composition (wt.%), and heat treatment conditions of the CdS samples prepared for this study.

2.2. Measurements

Optical absorption measurements were performed on a commercial spectrophotometer (Perkin Elmer 330). The samples were ground into a powder with a mean grain size of a few micrometers and dispersed in ethylene glycol for the absorption measurements.

Photoluminescence was obtained upon excitation at 350 nm from a Xe lamp. PL spectra were dispersed on a 1-m monochromator (Spex 1704) and detected by a photomultiplier tube (Hamamatsu R928). For variable temperature measurements between 20 K and room temperature, a closed-cycle cryogenic refrigerator was used. All reported spectra have been corrected for the instrumental response.

A transmission electron microscope (TEM, JOEL-100CX) operating at 100 kV was used to obtain TEM micrographs of CdS nanoparticles in both silica and sodium borosilicate glasses. Samples were fragmented, dispersed, and placed on perforated carbon microgrids for TEM sampling.

Table 1
Composition (wt.%), heat treatment conditions, and band edge absorption (nm) of prepared CdS samples

Label	SiO_2	B_2O_3	Na_2O	CdO	MnO	Treatment	Absorption
S1	95.5	–	–	4.5	–	150 °C/4 h/H_2S	450
S2	95.5	–	–	4.5	–	400 °C/4 h/H_2S	494
S3	93.0	–	–	5.0	2.0	400 °C/4 h/H_2S	453
S4	95.5	–	–	4.5	–	150 °C/12 h/H_2S 550 °C/12 h/vacuum	500
S5	93.0	–	–	5.0	2.0	150 °C/12 h/H_2S 550 °C/12 h/vacuum	479
B1	73.5	18.0	4.5	4.5	–	400 °C/4 h/H_2S	484
B2	71.4	17.6	4.5	4.5	2.0	400 °C/4 h/H_2S	437
B3	71.4	17.6	4.5	4.5	2.0	150 °C/12 h/H_2S 550 °C/12 h/vacuum	496

The value for the band edge absorption was determined from the first derivative of the absorption spectra (Fig. 3) [9] with a statistical error of about 5 nm for all of the samples.

3. Results

3.1. TEM characterization

TEM is commonly used to measure the sizes and size distributions of particles. The size and size distribution of CdS-doped glasses are affected by the heat treatment of the gels. A representative TEM micrograph of sample B3 is shown in Fig. 1. The micrograph demonstrates a random distribution in sizes of CdS nanoparticles in the borosilicate glass matrix. Fig. 2 shows the size distribution profile corresponding to the micrograph shown in Fig. 1. The average diameter of the CdS nanoparticles in sample B3 was ~9 nm.

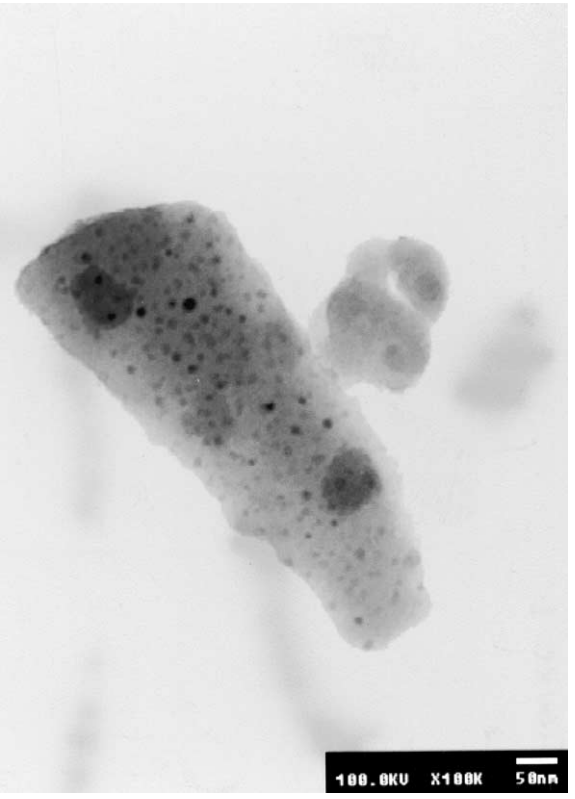

Fig. 1. TEM micrograph of sample B3 ($4.5Na_2O$–$17.6B_2O_3$–$71.4SiO_2$:4.5CdO:2.0MnO). The heat treatment conditions are given in Table 1.

3.2. Optical absorption

Room-temperature absorption spectra of the CdS-doped glass samples of this study are shown in Fig. 3. The approximate band edge absorption of CdS was obtained from Fig. 3 and is listed in Table 1.

As seen from Fig. 3, the absorption band edge of CdS is at a shorter wavelength relative to bulk samples of CdS. (The room temperature absorption band edges of bulk cubic-CdS and bulk wurtzite-CdS occur at approximately 2.31 eV (537 nm) and 2.38 eV (521 nm), respectively [23].) As the particle size decreases, the band gap of the nanocrystalline semiconductor shifts to higher energy. The shift to higher energy (Fig. 3) is attributed to the quantum size confinement effect [3, 24,25]. From Fig. 3, we also observe two additional features. First, undoped CdS has a longer wavelength absorption band edge in both silica and sodium borosilicate glasses treated at 400 °C. We therefore expected that the CdS materials with

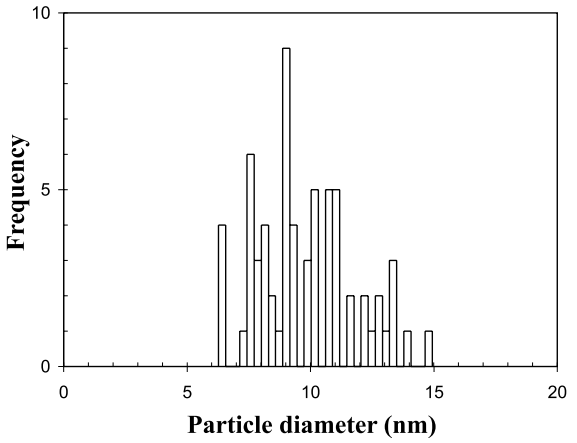

Fig. 2. Size distribution profile of sample B3 ($4.5Na_2O$–$17.6B_2O_3$–$71.4SiO_2$:4.5CdO:2.0MnO). The heat treatment conditions are given in Table 1.

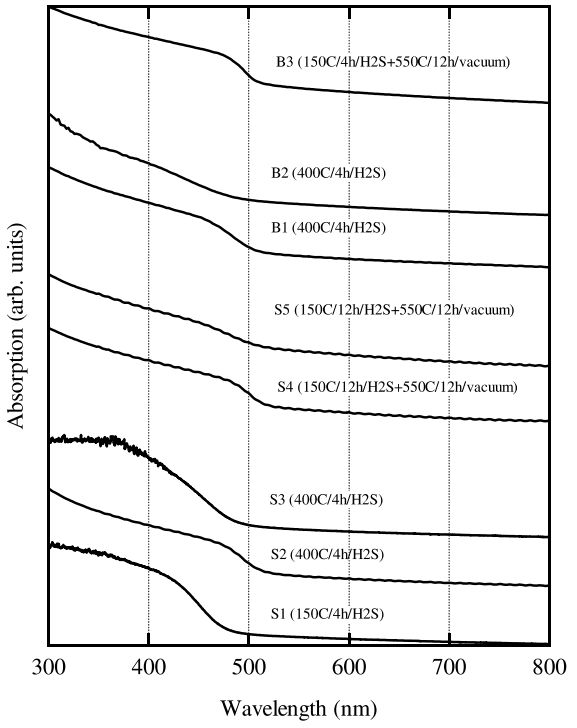

Fig. 3. Absorption spectra of CdS and CdS:Mn^{2+} nanoparticle materials at room temperature. The compositions and the heat treatment conditions of the samples are given in Table 1.

longer wavelength absorption band edges (Fig. 3) correspond to larger CdS nanoparticles. Second, in samples with the addition of Mn^{2+}, the CdS absorption band edge shifts to shorter wavelength. Levy et al. [24,26] observed a non-linear increase in the band gap of mixed $Cd_{1-x}Mn_xS$ nanocrystallites with increasing amounts of Mn. This effect is consistent with our observation of the blue shift of the CdS absorption band edge upon adding Mn.

3.3. Photoluminescence

Fig. 4 shows representative PL spectra of sample S1 at several temperatures upon broadband excitation at 350 nm. A PL band labeled by S (peaked at ~670 nm; ~1.85 eV) was observed at 20 K. The S band had a thermal quenching of intensity and decreased by a factor of ~9 between 20 K and room temperature.

Fig. 5 presents representative PL spectra of sample S4 at several temperatures upon excitation at 350 nm. The 20 K PL spectrum consists of a dominant band labeled SA (peaked at ~780 nm; ~1.59 eV) and a smaller narrower shoulder labeled A (peaked at ~526 nm; ~2.36 eV). The SA PL band was also thermally quenched similar to that observed for the S band of sample S1 and decreased by a factor of ~11 between 20 K and room temperature. The A band decreased in PL intensity and a red shift in band position with increasing temperature (from ~526 nm at 20 K to ~545 nm at room temperature) was observed.

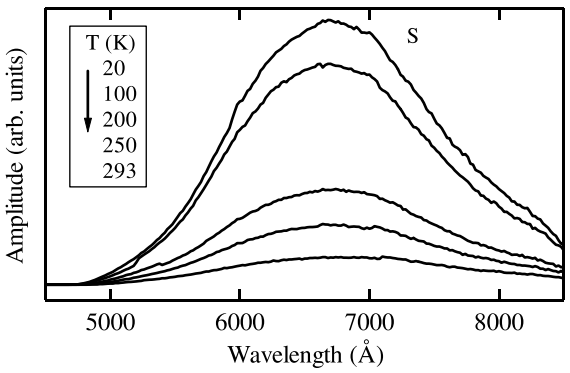

Fig. 4. PL spectra of sample S1 ($95.5SiO_2$–4.5CdO) at several temperatures upon excitation at 350 nm. The heat treatment conditions are given in Table 1.

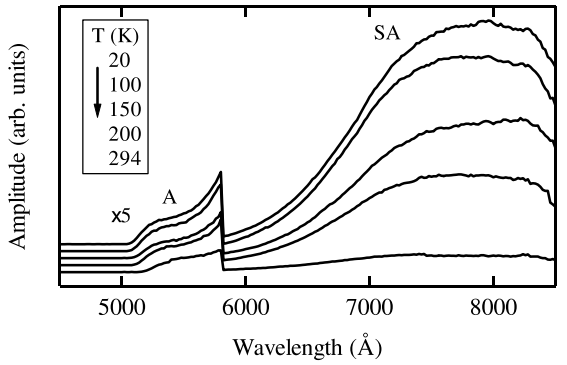

Fig. 5. PL spectra of sample S4 ($95.5SiO_2$–4.5CdO) at several temperatures upon excitation at 350 nm. The heat treatment conditions are given in Table 1.

Representative PL spectra of sample B3 at several temperatures are shown in Fig. 6. The 20 K PL spectrum consists of three bands labeled A (peaked at ~516 nm; ~2.40 eV), B (peaked at ~566 nm; ~2.19 eV), and C (peaked at ~716 nm; ~1.73 eV). Band A in this sample is similar in position and temperature dependence to band A in sample S4 (Fig. 5). Band B was quenched completely at ~130 K. Band C also exhibited thermal quenching of intensity and decreased by a factor of ~17 between 20 K and room temperature.

4. Discussion

A schematic depiction of the possible PL processes is given in Fig. 7. Initial band edge excitation promotes electrons from the valence band (VB) to the conduction band (CB) and consequently leaves holes in the VB. CB electrons and VB holes can directly recombine to emit in a zero-phonon or phonon-assisted process (process 1). When a CB electron is trapped by a shallow or deep donor-like trap, the trapped electron can recombine with a VB hole to emit a photon (process 2). When a VB hole is trapped by a shallow or deep acceptor-like trap, a CB electron can recombine with the trapped hole to emit a photon (process 3). Also, radiative recombination of an electron trapped by a donor and a hole trapped by an acceptor can occur (process 4). When a dopant ion like Mn^{2+} exists in the host lattice, mobile electron–hole pairs produced during the initial VB-to-CB excitation process can excite the dopant ion through an energy transfer process. This process leads to internal emission processes (e.g. d → d emission) characteristic of the dopant ion (process 5).

We attribute the A band (Figs. 5 and 6) to direct electron–hole recombination (process 1). The weak A band feature was observed in our samples. The energy of this band was dependent on the size

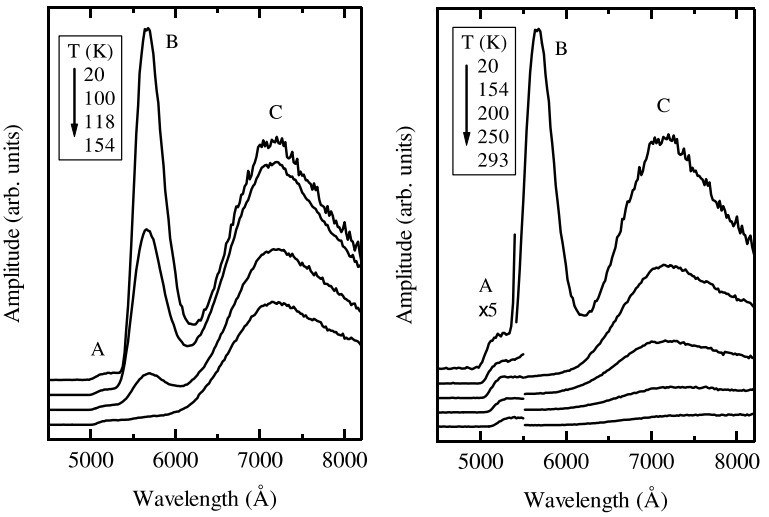

Fig. 6. PL spectra of sample B3 ($4.5Na_2O$–$17.6B_2O_3$–71.4 SiO_2 :4.5CdO:2.0MnO) at several temperatures upon excitation at 350 nm. The heat treatment conditions are given in Table 1.

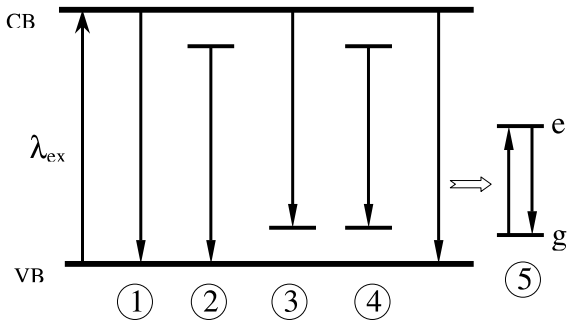

Fig. 7. Schematic depiction of possible PL processes upon band edge excitation. CB and VB represent the conduction band and the VB of the host, respectively. e and g represent the excited and ground states of a dopant ion, respectively.

of CdS nanoparticles and shifted to higher energy with decreasing size (for example, it occurs at ~526 nm in sample S4 with the band edge absorption of ~500 nm (Figs. 3 and 5) and as a high-energy shoulder below 500 nm in sample S1 with the band edge absorption of ~450 nm (Figs. 3 and 4)). The observed redshift of this band with increasing temperature (Figs. 5 and 6) is consistent with the redshift of the band gap (E_g) reported for bulk CdS with temperature ($dE_g/dT = -4.2 \times 10^{-4}$ eV/K [26]). Our observations support the assignment of the A band to direct electron–hole recombination.

It is commonly accepted [21,27] that the S band (Fig. 4) is due to the recombination of an electron trapped by a deep donor sulfur vacancy (V_S) state with a VB hole (process 2, Fig. 7) [21,27]. The thermal quenching of this band is due to thermal depopulation of electrons from the V_S traps to the CB. The process of thermal depopulation is governed by the activation energy between the donor-like trap state and the CB. The shallower the trap, the larger is the thermal quenching.

The SA band (Fig. 5) can in principle be attributed to one or more of processes 2–4 (Fig. 7). If process 2 or 3 were applicable, the deep donor-like or acceptor-like state would need to have a trap depth of at least 1 eV to account for the ~1.6 eV energy of the SA band. A trap depth of this magnitude is sufficiently large to prevent appreciable thermal quenching between 20 K and room temperature [28]. The thermal quenching observed for the SA band (Fig. 5), therefore, excludes processes 2 and 3 as the origin of the SA band. We consequently attribute the SA band to the donor–acceptor (D–A) pair recombination process (process 4). Xu et al. [29] observed a PL band at ~760 nm (1.63 eV) at 10 K in CdS nanoparticles (~100 nm size) synthesized by a hydrothermal colloidal process and proposed a D–A pair recombination model for the emission. They proposed that deep acceptor-like, self-activated Cd vacancy centers (V_{Cd}) form when S vacancy centers (V_S) are present above a threshold concentration. They argued that holes trapped by the Cd vacancy centers recombine with electrons trapped by the S vacancy centers to produce the ~760 nm PL band. The SA band observed in our samples is consistent with the donor (V_S)–acceptor (V_{Cd}) pair recombination model of Xu et al. [29] for the following reasons: (i) The energies of our SA PL band (~1.59 eV) and that of the D–A PL band of Xu et al. (1.63 eV) are similar; and (ii) our SA PL band and the D–A PL band of Xu et al. show similar thermal quenching. The simultaneous formation of S and Cd vacancies in our nanoparticle CdS samples could be due to vacuum heat treatment used in our preparation.

The thermal quenching observed for the B band in the PL spectrum of Mn^{2+}-doped samples (Fig. 6) indicates that it is due to a transition from a shallow donor state to the VB (or deep acceptor state), or a transition from the conduction band (or deep donor state) to a shallow acceptor state, or a transition from a shallow donor state to a shallow acceptor state. Transitions involving shallow states usually are thermally quenched because of the small activation barriers between shallow states and either the CB edge or VB edge. Since this PL band appeared only in Mn^{2+}-doped CdS samples and its PL intensity varied in the different samples (not graphically shown), the participating shallow states are presently uncertain, but are related to Mn^{2+}.

In Mn^{2+}-doped macroscopic and nanocrystalline CdS materials, it has been reported that isolated Mn^{2+} centers emit at ~580 nm in lightly doped samples [24,26] and paired Mn^{2+} centers emit at ~700 nm in doped samples with larger Mn concentrations [26]. Both the ~580 nm and ~700

nm emission bands are attributed [26] to a d–d transition between the $^4T_1$ excited state and the $^6A_1$ ground state of Mn^{2+}. Levy et al. [24] used mixed $Cd_{1-x}Mn_xS$ macroscopic and nanoparticle materials to study the PL of Mn^{2+} centers with increasing Mn^{2+} changing from isolated Mn^{2+} to paired. They found that the PL intensity of isolated Mn^{2+} centers reached a maximum at about $x = 0.1$ and that the PL band associated with paired Mn^{2+} centers became observable at about $x = 0.1$ and continued to increase in intensity as x was increased above 0.1. We attribute band C to the $^4T_1 \rightarrow {}^6A_1$ transition of paired Mn^{2+} centers in our Mn^{2+}-doped CdS nanoparticle samples ($x = \sim 0.44$) (process 5). We attributed the thermal quenching of band C (Fig. 6) to either a decreased energy transfer efficiency from the lattice to Mn^{2+} upon VB-to-CB excitation or increased non-radiative decay of the paired Mn^{2+} centers with increasing temperature.

5. Conclusions

The sol–gel process has been successfully applied to the preparation of CdS nanoparticles dispersed in SiO_2 and Na_2O–B_2O_3–SiO_2 glasses. We have established a quantitative effect of heat treatment conditions on the size and size distribution of the nanoparticles. Various photoluminescence processes of CdS and CdS:Mn^{2+} nanoparticle materials have been considered. Our present results will provide a useful foundation for further studies of undoped and doped $Cd_{1-x}Zn_xS$ and $CdS_{1-x}Se_x$ nanoparticle materials.

Acknowledgements

V.C.C. acknowledges financial support from Brazilian National Council of Research, CNPq. Acknowledgement is made to the donors of the Petroleum Research Fund, administered by the ACS, and the National Science Foundation for support of this research. We also thank Professor Rochel M. Lago from UFMG, Brazil, for his assistance in the H_2S heat treatment.

References

[1] H.M. Gibbs, G. Khitrova, in: H.M. Gibbs, G. Khitrova, N. Peyghambarian (Eds.), Nonlinear Photonics, Springer, Berlin, 1990 (Chapter 1).
[2] A.I. Ekimov, A.L. Efros, A.A. Orushchenko, Solid State Commun. 56 (1985) 921.
[3] R.N. Bhargava, D. Gallenger, X. Hong, A. Nurmikko, Phys. Rev. Lett. 72 (1994) 416.
[4] A.P. Alivisatos, J. Phys. Chem. 100 (1996) 13226.
[5] Y. Wang, Acc. Chem. Res. 24 (1991) 133.
[6] M.Y. Han, L.M. Gan, W. Huang, C.H. Chew, B.S. Zou, Chem. Lett. 8 (1997) 751.
[7] A.P. Alivisatos, Science 271 (1996) 933.
[8] J.D. Mackenzie, Y.H. Kao, in: S. Iraj Najafi (Ed.), Glass Integrated Optics and Optical Fiber Devices, Proc. SPIE CR53, 1994.
[9] M.P. Pileni, Catal. Today 58 (2000) 151.
[10] Y. Fuyu, J.M. Parker, Mater. Lett. 6 (1988) 233.
[11] G. Counio, T. Gacoin, J.P. Boilot, J. Phys. Chem. B 102 (1998) 5227.
[12] Y. Wang, N. Heron, K. Moller, T. Bein, Solid State Commun. 77 (1991) 33.
[13] R.N. Bhargava, J. Lumin. 70 (1996) 85.
[14] N. Murase, R. Jagannathan, Y. Kanematsu, M. Watanabe, A. Kurita, K. Hirata, T. Yazawa, T. Kushida, J. Phys. Chem. B 103 (1999) 754.
[15] Y. Wang, A. Suna, M. Mahler, R. Kasowski, J. Phys. Chem. 87 (1987) 7315.
[16] P. Rossetti, R. Hull, J.M. Gibson, L.E. Brus, J. Chem. Phys. 82 (1985) 552.
[17] L. Brus, J. Phys. Chem. Solids 59 (1998) 459.
[18] M.P. Pileni, J. Phys. Chem. 97 (1993) 6961.
[19] P. Lianos, J.K. Thomas, Chem. Phys. Lett. 125 (1986) 299.
[20] N. Nogami, K. Nagasaka, J. Non-Cryst. Solids 147 (1992) 331.
[21] B. Liu, G.Q. Xu, L.M. Gan, C.H. Chew, W.S. Li, Z.X. Shen, J. Appl. Phys. 89 (2001) 1059.
[22] K. Misawa, H. Yao, T. Hayashi, T. Kobayashi, J. Cryst. Growth 117 (1992) 617.
[23] L.I. Berger, Semiconductor Materials, CRC, New York, 1997, p. 199.
[24] L. Levy, D. Ingert, N. Feltin, M.P. Pileni, J. Cryst. Growth 184&185 (1998) 377.
[25] M.T. Wilson, C.Y. Li, J.D. Mackenzie, N.M. Haegel, Nanostruct. Mater. 2 (1993) 391.
[26] L. Levy, N. Feltin, D. Ingert, M.P. Pileni, J. Phys. Chem. B 101 (1997) 9153.
[27] N. Chestnoy, T.D. Harris, R. Hull, L.E. Brus, J. Phys. Chem. 90 (1986) 3933.
[28] D.R. Vij, N. Singh, Luminescence and Related Properties of II–VI Semiconductors, Nova Science, Commack, NY, 1998.
[29] G.Q. Xu, B. Liu, S.J. Xu, C.H. Chew, S.J. Chua, L.M. Gana, J. Phys. Chem. Solids 61 (2000) 829.